SciencePG

Science Publishing Group

Review Article

Spin-Orbit Induced Dynamics in Multilayer Nanostructures

Andrii Korostil[*], Mykola Krupa

Institute of Magnetism of National Academy of Sciences of Ukraine, Kyiv, Ukraine

Email address:

amand@rambler.ru (A. Korostil), krupa@imag.kiev.ua (M. Krupa)

[*]Corresponding author

Abstract: Features of the current spin-orbit induced magnetic dynamics in multilayer nanostructures with nonmagnetic heavy metal layers possessing by a strong spin-orbit interaction are studied. These structures include ferromagnetic (F) (antiferromagnetic AF)/normal metal (N) nanostructures based on both conductive and insulating magneticsand heavy normal metals (e. g., FeCoB/Ta, YIG/Pt, Nio/Pt). The spin Hall effect of the conversion of an incoming charge current into a transverse (with respect to the charge current) spin current induces a spin-transfer torque and magnetic dynamics including a magnetic precession and switching. The magneto-dynamic effect of a spin current pumping generation together with the inverse spin Hall effect of conversion of the spin current into the incoming charge current provide the influence of the magnetic dynamics on the incoming charge current. These feedforward and feedback between the incoming charge current and the magnetic dynamics can be the basis for the spin-orbit driven self-sustained auto-oscillations of a magnetic order in the nanostructures. It is shown that the considered magnetic nanostructures possess by properties of controlled microwave radiation attaining tens THz in the antiferromagnetic case. Magnetic-induced changes of the electric resistance in the mentioned nanostructure are considered.

Keywords: Magnetic Nanostructures, Magnetic Dynamics, Spin Currents, Spin Hall Effects, Feedback, Nano-Oscillations

1. Introduction

There is much current interest in dynamical processes in magnetically ordered systems both from scientific and technological viewpoints. The special interest is related to the problem of the intercoupling between a spin-polarized electron current and the magnetic dynamics in multilayer magnetic nanostructures that can be exhibited in such phenomena, as magnetic switching and a sustained precession of magnetic order vectors

The interrelation between the spin-polarized current and magnetic order vectors in magnetic multilayer nanostructures [1-3], permitting their mutual control [4], constitutes the basis of the operation of novel nano-devices [5], some of them with properties of a magnetic random-access memory (MRAM) [6], magnetic logic and coherent microwave radiation sources that presents considerable fundamental and application interest [7, 8]. The operation of these devices can be based on both the spin-polarized current-induced and the

current spin-orbit-induced magnetic dynamics including magnetic switching and precessing [9-11]. Such phenomena have real potential for application in systems of high-speed magnetic processing information and high frequency fine-tuned GHz and THz electromagnetic radiation.

The intercoupling between a spin current and magnetic state in magnetic nanostructures constitutes the basis of the current-induced manipulation by magnetic dynamics and vice-versa, i.e. the magnetic state-induced manipulation by the spin current [12-15]. The spin current can be converted from an incoming charge current under internal effective magnetic fields of interactions of a different origin (including *s-d* exchange and spin-orbit interactions) with corresponding features of the action of a spin torque on the magnetic states and their dynamics. Inducing magnetic dynamics such the spin torque can causes switching and precession of the magnetic order vectors (including ferro- and

antiferromagnetic orders) in magnetic nanolayers with ferromagnetic (FM) and antiferromagnetic (AF) interactions. The frequency of the magnetic dynamics is determined by the magnitude of magnetic exchange interaction, which is the largest for antiferromagnetic materials. The prospect of obtaining the technological magnetic nanostructures with low threshold incoming currents, low power consumption and controlled high frequency operation is related to utilization of the spin-orbit effects of the spin polarization and magnetic nanostructures with AF exchange interactions.

Generally, the spin-orbit interaction includes the bulk spin Hall effect (SHE) [12, 13] of the transverse (relatively to an incoming current) deflection of electrons with opposites spins in opposite sides and the interface (two-dimensional) Rashba spin-orbit(RSO) effect [14, 15] of the spin splitting of an electron disperse along an electron wave vector. The impact of the spin current on the magnetic states realizes via the spin torque T consisting of so-called a field-like and dumping-like part $T_{\parallel}$ and $T_{\perp}$, respectively, which are related to the effects of magnetic order switching and precession dumping or antidumping. The field-like torque $T_{\parallel}$ originates predominantly by the spin-orbit coupling at the interface in combination with the perturbation of the electron distribution function. The torque $T_{\perp}$ originates predominantly by the perturbation of electronic states by the applied electric field.

The current spin-orbit controlled microwave magnetic dynamics is realized for nanostructures composed of a heavy metal nanolayer (for instance, Pt, Ta) possessing by the strong enough spin-orbit interaction and the adjacent active magnetic nanolayerwith a strong exchange interaction attaining maximum values of the order of tens THz in the AF cases. For multisublattice magnetic structures (for instance, for AF) a general magnetic dynamics is a combined effect of dynamics of each of magnetic sublattices coupled by the strong exchange interaction.

The interconnection between the incoming charge current and magnetic dynamics occurs in the mentioned case via the spin current and the spin transfer effect for the each sublattice singly. In such the magnetic systems the simultaneous action of SHE and the inverse SHE (of the transverse to spin current charge current) results in the feedback between the incoming charge current and the magnetic dynamics. This provides sustained steady-state spin torque magnetic oscillations, convertible via a magnetoresistance effect into an ac voltage and the current-driven high frequency radiation.

The paper is organized as follows. In section 2, the conversion of an incoming current into the spin currentunder internal effective bias fields of the exchange interactions of a different origin in magnetic nanostructures is studied. In Section 3, the spin and charge density diffusions in the bilayer magnetic structures with the strong spin-orbit interaction are considered in the framework of nonlinear kinetic leading to renormalization of parameters of a magnetic precession. Section 4 is devoted to dynamic feedback in F/SH nanostructures. It is shown that spin pumping and spin transfer torques as two reciprocal

processes result in a dynamical feedback effect interconnecting energy dissipation channels of both magnetization and current. In Section 5, features of spin pumping and spin-transfer torques as two reciprocal phenomena are considered in AF based nanostructures. In Section 6, the current-induced magnetic dynamics is considered in the bilayer nanostructures composed of an insulating AF and adjusted heavy normal metal with the SHE.

2. The Spin Polarization and Spin Current

The electric control of the magnetic dynamics in the mentioned magnetic nanostructures occurs through the exchange interaction between the spin current and a localized magnetic order. The spin current induces the spin torque causing magnetic dynamics in the form of the precession or switching of the magnetization in Fs and AF order in AFs [16-18]. The magnitude of the spin torque is determined by the mechanism of the conversion of incoming charge current into the spin current interacting with the magnetic order via an exchange interaction. The conversion of the incoming electric current into spin polarization state in the ferromagnetic nanostructures can be produced by the effective bias field of the *s-d* exchange interaction in the magnetic layer acting as a spin polarizer. The spin polarization occurs as the results of the spin splitting of the electron band spectrum on the two branches with and without their intersection by the Fermi level (Fig. 1) (see [11]) that correspond two (Fig. 1b) and single (Fig. 1c) channel conductions of the electrons with different spin projections relatively to the magnetization.

In the usual two-channel case, the majority electros with the spin projection parallel to the magnetization, occupy the one conduction channel and the minority electrons with the antiparallel spin projection occupy the another conduction channel. This results in the incomplete spin polarization of the electric current. In the single-channel case, which is realized for magnetic semimetals [11], the conduction electrons with the fixed spin projection occupy only one conduction band and the incoming current converts into the pure spin current. The impact of the polarized electric current on the magnetization occurs through the exchange interaction between the corresponding spin polarized current and the controlled localized spins. The passage of the spin-polarized current into the controlled magnetic nanolayer causes the spin torque exerting the magnetization switching or precession.

In the mentioned case, the transfer electron charges into the controlled magnetic layer results in thermal losses and increase of a power consumption. This imposes restrictions on contact sizes, which have to provide the threshold density of the spin current subject to the condition that the electric current does not exceed the value of an electrical breakdown.
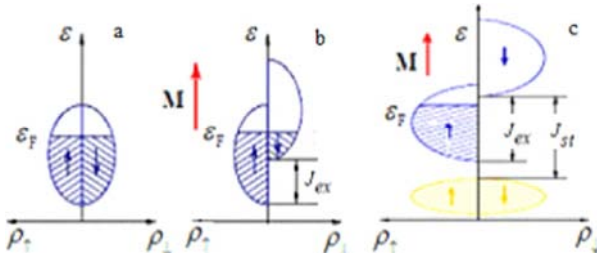
Figure 1. *Scheme of the spin-splitting of the band spectrum induced by the exchange interaction J_{ex}, where $\rho_\uparrow$ and $\rho_\downarrow$ are the densities of electron states with different spin projections ($\uparrow,\downarrow$), (a), (b) and (c) are normal metal, ferromagnetic metal and ferromagnetic semimetal, respectively; **M** is the magnetization vector.*

These problems can be avoided by the utilizing the spin-orbit interaction for the spin polarization. In this case, the exchange interaction of the spin current with the localized spins is provided without passage of the charge current in the magnetic nanolayer [1, 3, 4].

The spin-orbit interaction in the two-dimensional systems with of the broken structure inversion symmetry, known as the Rashba spin-orbit interaction [1-3], is realized in the interfaces of the magnetic nanostructures with two-dimensional electron properties and an interfacial potential drop. In a single-electron approximation, this interaction is described by the two-dimensional expression for a quasi-relativistic correction [2]. Taking into account the electric field $\mathbf{E} = E_z \cdot z$ along growth direction z, the corresponding Rashba Hamiltonian can be represented as

$$H_R = \boldsymbol{B}_R \boldsymbol{\sigma}, \quad \boldsymbol{B}_R = \left(\frac{\alpha_R}{\hbar}[z \times \boldsymbol{p}] \right) \qquad (1)$$

where $\alpha_R \sim E_z$ is the Rashba parameter, $\boldsymbol{B}_R$ is the effective Rashba magnetic field which is dependent on the electron momentum $\boldsymbol{p}$ and σ is the vector of the Pauli spin matrices. The system (1) describes the characteristic properties of the Rashba spin-orbit interaction, although in realistic systems, the broken inversion symmetry causes distorts of the free electron wave functions near to atomic nuclei and consequently, it changes a spin-orbit interaction [1, 2]. Due to (1), the effective Rashba field $\boldsymbol{B}_R$ exerts the spin precession of the conduction electrons. In addition, one leads to the symmetric spin splitting of the single-electron dispersion along the conduction electron momentum that experimentally observed in interfaces of magnetic nanostructures (Fig. 2).
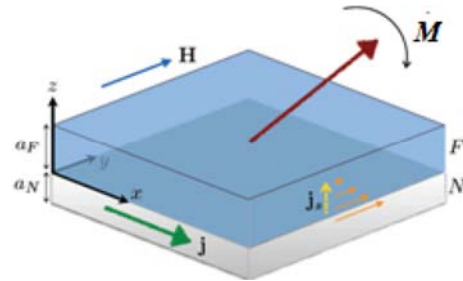
The spin-polarized electric current lies in the plane of the magnetic layer and one does not pass in the normal direction. Its interaction with the localized magnetization occurs through s-d-exchange interaction of the form $H_{sd} = J_{sd} \boldsymbol{S} \cdot \sigma$, where $J_{sd} \sim J_c$, where J_c is the input electric current and $\boldsymbol{S}$ is the localized spin. Thereby, the change of the incoming electric current results in the corresponding change of the magnetization. The application of an electric field along the vector z results in changes of the Rashba parameter and magnetization dynamics, which is restricted by the magnetization switching.

The spin polarization of the electric current can be caused also by SHE [12, 13], in which the passage of the electric current through heavy metal (for instance, Pt, Ta) with the strong spin-orbit interaction exerts the spin dependent transverse deviation of the electric current and the transverse pure spin current. The spin orientation of the latter is perpendicular to the electric current and the interface normal (Fig. 3). The electric current lies in the plane of the adjacent heavy metal nanolayer and do not pass into the magnetic nanolayer. This avoids the mentioned constraints on contact sizes in the magnetic nanostructure and leads to reduction of the threshold current densities and the energy consumption.
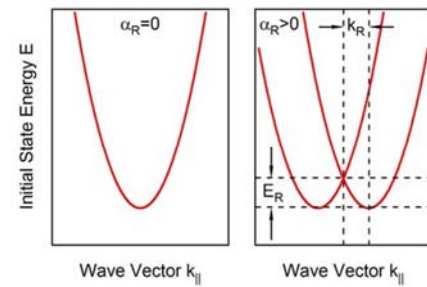
Figure 2. *The dispersion of the two-dimensional electron gas planar momentum vector $k_\parallel$; a_R is the Rashba parameter, k_R is previous to(on the left) and after (on the right) action of the Rashba spin-orbit interaction causing the spin-splitting along of the offset away from $k_\parallel = 0$ of the spectral curve to the initial position.*

Figure 3. *SHE of the spin-orbit conversion of the input electric current $\boldsymbol{j}$ into the spin current $\boldsymbol{j}_s$ with the spin polarization denoted by arrows along the $\boldsymbol{y}$ axis in the two-layered magnetic nanostructure. The spin current exerts on the magnetization $\boldsymbol{M}$ of the magnetic layer, $\boldsymbol{H}$ is external magnetic field.*

The reciprocal of the SHE is the inverse spin Hall effect (ISHE), i.e. the conversion of an injected spin current into a traverse electric current or voltage. The SHE generates spin currents and spin accumulations.

Together with the spin pumping effect originated from magnetic dynamics, SHE and ISHE provide the interconnection between the magnetic dynamics and the electric current. While the SHE generates spin currents and spin accumulations, the ISHE detects spin currents and can generate the spin-based electric power (see [3, 12, 13]).

The additional transverse momentum component $p_{\sigma\perp}$ in the spin Hall effect is proportional to the derivative of the spin-orbit interaction $H_{so} = \beta [\nabla V \times \boldsymbol{p}] \boldsymbol{\sigma}$ with respect to the

momentum p, i.e. $p_{\sigma\perp} \sim \beta$ (see [13]). The solution of the corresponding Schrödinger Hamiltonian with the spin-orbit interaction gives that the action of the latter on the conduction electrons is equivalent to the action of the effective spin-dependent Lorentz force $F_\sigma \sim [v \times B_\sigma]$, where v is the electron velocity, and $B_\sigma = [\nabla \times A_\sigma]$ is the spin-dependent effective magnetic field. Here, $A_\sigma \sim [\nabla \times E_{tot}]$ is the effective magnetic potential with E_{tot} being the total electric field [13]. The effective field B_σ causes the transverse deviation of the electric current with generation of the transverse spin current. The charge current passes along the heavy metal nanolayer and the generated spin current passes into the controlled magnetic layer where owing the exchange interaction through the torque changes the magnetization dynamics. This can lead to the magnetization precession or switching.

Features of the electron transport in the mentioned magnetic nanostructures are related to the spin dependent scattering on interfaces. The electron scattering on the normal metal (N)/magnetic metal (M) interface represents the special interest for magnetic heterostructures with the strong spin-orbital interaction and SHE. In the ferromagnetic case, by scattering theory [19], the spin current $j_s^{(N|F)}$ through an N|F interface (on the N side, flowing into F) can be expressed in terms of the F magnetization M and the (vector) spin accumulation μ_{sN} in N:

$$j_{sN}(m) = (j_\uparrow - j_\downarrow)m - \frac{1}{e}\left(G_r m \times (m \times \mu_{sN}) + G_i (m \times \mu_{sN})\right) \qquad (2)$$

where $m = M/|M|$, $e = -|e|$ is the electron chargeand

$$j_{\uparrow(\downarrow)} = \frac{G_{\uparrow/\downarrow}}{e}\left[(\mu_{cN} - \mu_{cF}) \pm (m \cdot \mu_{sN} - \mu_{sF})\right] \qquad (3)$$

is the flow of electrons with spin-up and down along m driven by the difference between effective charge chemical potentials in N and F $(\mu_{cN} - \mu_{cF})$ and the difference between spin accumulations at both sides of the interface $(m \cdot \mu_{sN} - \mu_{sF})$.
The spin-dependent conductance at the interface

$$G_{\uparrow(\downarrow)} = G_0 \sum_{nm}\left[\delta_{nm} - |r_{nm}^{\uparrow(\downarrow)}|^2\right] \qquad (4)$$

where $G_0 = e^2/\hbar$ is the conductance quantum, related to the spin-dependent reflection coefficient $r_{nm}^{\uparrow(\downarrow)}$ corresponding to the electron transition between quantum states n and m in with spin projections $\uparrow$ and $\downarrow$, respectively, in N. Conductance G_r and G_i in (4) are determined as real and imaginary parts of the spin-mixing conductance

$$G_{\uparrow\downarrow} = G_0 \sum_{nm}\left[\delta_{nm} - (r_{nm}^\uparrow)(r_{nm}^\downarrow)^*\right] \qquad (5)$$

i.e., $G_{r(i)} = \text{Re(Im)}G_{\uparrow\downarrow}$ is related to spin-flip electron scattering at the interface.

Due to (4), the longitudinal component of the spin current cal flow in a metallic magnetic.Its transverse components are absorbed causing at the interface the spin-transfer torque (STT)

$$T_{STT} = \frac{\hbar}{2e} m \times (m \times j_s^{(N|F)}) \qquad (6)$$

acting on the magnetic exerting on the magnetic dynamics.

Specially, large STT is realized in the current-in-plane (CIP) configuration with the spin current generated by the SHE [20-21] in the N layer and converted to a magnetization torque by the exchange interaction at the interface. This contributes a so-called "damping-like" torque proportional to G_r with symmetry identical to the exchange-mediated term, and a "field-like" torque proportional to G_i. The mentioned spin-orbit induced torque on the magnetic states in a normal metal has potential applications in spintronics including magnetic storage and communication technology.

3. Robustness of Ferromagnetic Dynamics

In ferromagnet/normal metal heterostructures, spin pumping and spin-transfer torques are two reciprocal processes that occur concomitantly. Their interplay introduces a dynamic feedback effect interconnecting energy dissipation channels of both magnetization and current. The solution of the spin diffusion process in the presence of the SHE in the NM shows that the dynamic feedback gives rise to a nonlinear magnetic damping that is crucial to sustain uniform steady-state oscillations of a spin Hall oscillator [23-25].

In ferromagnet (FM)/normal metal (NM) heterostructures, nonlocal effects arise because conduction electrons and magnetization reside in different materials and couple only at the interface. In this regime, spin pumping plays the role of spin electromotive force (SMF), which refers to the generation of spin current from a precession FM into the NM [25]. The pumped spin current is accompanied by a backflow of spin current [24, 25], which reacts on the FM through the spin transfer torque (STT). The combined effect of spin pumping and backflow-induced STT renormalizes the spin-mixing conductance at the interface [17, 23]. However, in the presence of the SHE, spin pumping and spin backflow are also connected by the combined effect of the SHE and its inverse process ISHE, which forms a feedback loop as illustrated in Fig. 4.

This additional feedback mechanism, proportional to the SH angle squared, θ_s^2, that is essential to the electron transport in FM/NM heterostructures. Consequently, this feedback effect is important to the magnetization dynamics. In a reciprocal sense, if we apply an ac current density to the NM, the SHE will drive the magnetization precession via the STT, which in turn can pump spin current back into the NM and renormalize the resistivity by means of the ISHE.

The feedback effect qualitatively modifies the dynamical behavior of an FM/NM heterostructure. The feedback

manifests as a novel nonlineardamping effect inthe magnetization dynamics. It enables uniform auto-oscillations
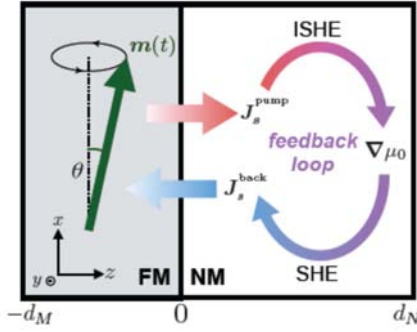
Figure 4. *In a FM/NMS bilayer, spin pumping and backflow are connected by the SHE and its inverseprocess (ISHE).*

of a spin Hall oscillator and prevents magnetic switching. The feedback effect gives rise to a spin Hall magnetoimpedance in the electron transport, which reduces to the observed SMR in the dc limit.

Consider a FM/NM bilayer structure represented in Fig. 4 with the layer thicknesses are d_M and d_N, respectively. The coordinate system is chosen such that the magnetization direction at rest is along x, and the interface normal is along z. It is assumed that the FM is insulating (e.g., YIG), but the essential physics remains valid for a conducting FM since the feedback process takes place only on the NM side.

In terms of the electrochemical potential $\mu_0 / 2$ and the vector of spin accumulation μ in the NM, the charge and spin current densities J_i^c and $J_{(ij)}^s$, respectively, are described by the expression $J_{i(ij)}^{c(s)} = -\frac{\sigma}{2e}\left(\partial_i \mu_{0(j)} \pm \theta_s \varepsilon_{ijk} \partial_{j(k)} \mu_k(0)\right)$ with the transport direction i, the spin polarization direction j, the conductivity σ and the electron charge e. In given device geometry, only the spin current flowing along z-direction is relevant, and so $\mu = \mu(z,t)$. Correspondingly, the spin (charge) current density reduces to a vector $J_{z(c)}$. The electron and spin dynamics in the NM are described by equations

$$\frac{\partial \mu}{\partial t} = D\frac{\partial^2 \mu}{\partial z^2} - \frac{1}{\tau_{sf}}\mu \tag{7}$$

$$J_c = -\frac{\sigma}{2e}\left[\nabla\mu_0 + \theta_s z \times \frac{\partial \mu}{\partial z}\right] \tag{8}$$

$$J_s = -\frac{\sigma}{2e}\left[\frac{\partial \mu}{\partial z} + \theta_s z \times \nabla\mu_0\right] \tag{9}$$

Where D is the diffusion constant, τ_{sf} is the spin-flip relaxation time.

To solve the spin accumulation μ, we assume that the charge current density J_c is fixed by external circuit and is uniform in space. Besides that, we have two boundary conditions $J_s(d_N) \equiv J_{s0} = 0$ and

$$J_{s0} = \frac{G_r}{e}\left[m \times (m \times \mu_{s0}) + \hbar m \times \dot{m}\right] \tag{10}$$

where $\mu_{s0} = \mu(0)$ and G_r is the real part of the areal density of the spin-mixing conductance (the imaginary part is the real part of the areal density of the spin-mixing conductance (the imaginary part G_i is neglected since $G_r \gg G_i$). On the right hand side of (10), the first term is the STT and the second term is the spin pumping. They are two fundamental ingredients bridging the electron (spin) transport in the NM with the magnetization dynamics of the FM. Due to the conservation of spin angular momentum, the spin current density J_{s0} is absorbed by the FM, which is reflected by the Landau-Lifshitz-Gilbert (LLG) equation

$$\frac{dm}{dt} = \gamma H_{eff} \times m + \alpha_0 m \times \frac{dm}{dt} + \frac{\hbar \gamma_{ex}}{2eM_s d_M} J_{s0} \tag{11}$$

where γ is the gyromagnetic ratio, $\hbar$ is the reduced Planck constant, M_s is the saturation magnetization, α_0 is the Gilbert damping constant, and H_{eff} is the effective magnetic field.

For typical FMs, the magnetization dynamics is much slower than the spin relaxation rate in the NM so that $\omega \tau_{sf} \ll 1$. In this limit, the spin accumulation $\mu(z,t)$ adapts to the instantaneous magnetization orientation and is kept quasi-equilibrium. As a result, the spin dynamics described by (7) reduces to a stationary spin diffusion process at any specified time. Retaining to second order in θ_s^2 in (7) gives

$$\mu(z) = \frac{2e\lambda}{\sigma}\left\{\theta_s \Lambda_1(z) z \times J_c + \Lambda_2(z)\left[J_{s0} + \theta_s^2 z \times (z \times J_{s0})\right]\right\} \tag{12}$$

where $\lambda = \sqrt{D\tau_{sf}}$ is the spin diffusion length, $\Lambda_1(z) = \sinh A(z) / \cosh A(0)$, $\Lambda_2(z) = \cosh B(z) / \sinh B(0)$ with $A(z) = (2z - d_N) / 2\lambda$ and $B(z) = (z - d_N) / \lambda$. Here, it is suppressed the t variable in $\mu(z)$ since its time dependence simply originates from J_c and J_{s0}. Combining (7)−(12) results in either eliminate the electron degrees of freedom (J_c and J_{s0}) to derive an effective dynamics of the magnetization, or eliminatethe time derivative of the magnetization to get an effective magneto-transport of the electrons. These operations amount to invoking the dynamic feedback mechanism.

Assume that J_c is an applied dc charge current density. Then the total spin current density J_{s0} flowing into the FM in terms of the magnetization $m(t)$, by which the LLG(10) will no longer involve any electron degrees of freedom, and the feedback effect is thus implemented mathematically. To this end, we combine (9) and (11) which gives two convoluted relations of J_{s0} and μ_{s0}. By means of iterations truncating at θ_s^2 order, we can solve J_{s0} as a function of J_c, $m(t)$ and its time derivative. Then we insert this J_c into (10), which yields the effective magnetization dynamics

$$\frac{d\boldsymbol{m}}{dt} = \gamma \boldsymbol{H}_{eff} \times \boldsymbol{m} + \omega_s \boldsymbol{m} \times [(z \times \boldsymbol{j}_c) \times \boldsymbol{m}] + (\alpha_0 + \alpha_{sp})\boldsymbol{m} \times \frac{d\boldsymbol{m}}{dt} + \alpha_{rb}\left(m_z^2 \boldsymbol{m} \times \frac{\partial \boldsymbol{m}}{\partial t} + \frac{\partial m_z}{\partial t} \boldsymbol{m} \times z \right) \qquad (13)$$

where $\boldsymbol{j}_c$ is the unite vector of $\boldsymbol{J}_c$ and

$$\omega_s = \theta_s J_c \frac{\hbar\gamma}{eM_s d_M} \frac{\lambda G_r \tanh\frac{d_s}{2\lambda}}{\sigma + 2\lambda G_r \coth\frac{d_s}{\lambda}} \qquad (14)$$

is the strength of the STT (driven by $\boldsymbol{J}_c$) scaled in the frequency dimension. The two damping coefficients are described by the expression

$$a_{sp(fb)} = \frac{(\lambda\theta_s^2\beta)^{0(1)}\hbar^2\gamma}{2e^2 M_s d_M} \frac{\sigma G_r}{(\sigma + 2\lambda G_r \beta)^{1(2)}} \qquad (15)$$

where $\beta = \coth(d_N / \lambda)$. Here, a_{sp} describes the conventional enhanced damping from spin pumping with the spin backflow effects taken into account [25]; it is independent of the SHE. By contrast, the a_{rb} term reflects the dynamic feedback realized by virtue of the combined effect of the SHE and its inverse process as schematically shown in Fig. 4. From (13), it is we see that this damping term is nonlinear in $\boldsymbol{m}_\perp$: the component of $\boldsymbol{M}$ transverse to the effective field H_{eff}, the Gilbert damping term is linear in $\boldsymbol{m}_\perp$.

The feedback-induced nonlinear damping effect can be explained in the following way. If the magnetization precession is getting larger, it will trigger a chain reaction: first, the pumped spin current $\boldsymbol{J}_{s0}$ increases, then the spin diffusion becomes stronger (i.e., $|\partial_z \boldsymbol{\mu}_s|$ gets larger). This will necessarily lead to a larger $\nabla\mu_0$ in the NM according to (8). Finally, the change of the emf will feed back into $\boldsymbol{J}_{s0}$ according to (9), preventing its further increase. Therefore, the growing magnetization precession is inhibited. The entire process realizes a negative feedback and respects Lenz's law.

4. Spin Currents in AF Nanostructures

The spin pumping and spin-transfer torque in AF based nanostructures represent the combined effect of their action in each of magnetic sublattices of the AF coupled by a strong exchange interaction. Magnetization dynamics of these coupled sublattices leads to an AF order ($\boldsymbol{l}$) dynamics manifesting as precession and switching. Similarly, to the magnetization in the ferromagnetic case, the AF order precession generates the spin pumping current, which via the ISHE in adjacent nonmagnetic nanolayers can converts into the transverse charge current. Thereby, the influence of the AF dynamics on the charge current in AF nanostructures is realized [26]. The inverse impact of the charge current on the AF precession is realized via the spin Hall effect of the conversation of the charge current into the transverse spin current which owing to the exchange interaction exerts the spin transfer torque on the AF order precession.

Characteristic features of the AF dynamics and its interconnection with the spin currents in the form of the precession-induced spin pump and spin transfer torque is manifested in the AF two-sublattice model with an easy axis directed along the axis z, and magnetization unite vectors $\boldsymbol{m}_1$ and $\boldsymbol{m}_2$. These vectors are driven by the exchange interaction, the anisotropy, and a magnetic field in the z direction. In units of frequency, they are represented by ω_E, ω_A, and $\omega_H = \gamma H_0$, respectively. The equations of motion in a free precession approximation are

$$\dot{\boldsymbol{m}}_1 = \boldsymbol{m}_1 \times [\omega_E \boldsymbol{m}_2 - (\omega_E + \omega_H)z],$$
$$\dot{\boldsymbol{m}}_2 = \boldsymbol{m}_2 \times [\omega_E \boldsymbol{m}_1 - (\omega_E - \omega_H)z], \qquad (16)$$

where the effective field causing the magnetization precession in a magnetic sublattice contains the contribution from the exchange interaction with an adjacent magnetic sublattice. In linear response, when $\boldsymbol{m}_{1(2)} = z + \boldsymbol{m}_{1(2)\perp}\exp(i\omega t)$ at $|\boldsymbol{m}_\perp| \ll 1$ the resonance frequencies are then

$$\omega = \omega_H \pm \omega_R = \omega_H \pm \sqrt{\omega_A(\omega_A \pm 2\omega_E)} \qquad (17)$$

where the two corresponding eigenmodes are characterized by different chiralities. The left-handed (right-handed) mode, both $\boldsymbol{m}_1$ and $\boldsymbol{m}_2$ undergo a circular clockwise (counterclockwise) precession with π phase difference. In the absence of magnetic field, viz. $\omega_H = 0$, the two modes are degenerate.

Since without the AF interaction, spin current pumped from each of two magnetic sublattices is proportional to $\boldsymbol{m}_{1(2)} \times \partial_t \boldsymbol{m}_{1(2)}$, the total pumped spin current is roughly proportional to $\boldsymbol{l} \times \partial_t \boldsymbol{l}$, where $\boldsymbol{l} = (\boldsymbol{m}_2 - \boldsymbol{m}_1)/2$ denotes the staggered field.

The cone angles of $\boldsymbol{m}_1$ and $\boldsymbol{m}_2$ are different: in the left-handed (right-handed) mode, $\theta_2/\theta_1 = \eta$, where $\eta \approx (1 + \sqrt{\omega_A/\omega_E})^2$, so that a small magnetization $\boldsymbol{m} = (\boldsymbol{m}_1 + \boldsymbol{m}_2)/2$ is induced in the AF dynamics state.

The spin currents in AF nanostructure determined by mixed scattering channels associated with different sublattices on a N/AF. Typical AF materials are insulators and incident electrons from the normal metal cannot penetrate far. Only a single atomic layer of AF directly connected to N suffices to describe the dominant contribution to interface scattering. Therefore, the essential physics is captured by modeling the N/AF interface as being semi-infinite in the transport direction and infinite in the transverse direction.

In the nearest-neighbor tight-binding model on a cubic lattice, in terms of the ratio the scattering matrix in the linear approximation in the small m is described by the expression

$$S = S_0 + S_\varpi \tau_1 \sigma_0 + \Delta S[\tau_3(l \cdot \sigma) + \tau_0(m \cdot \sigma)] \qquad (18)$$

where $\tau_{1,2,3}$ are pseudospin Pauli matrices for sublattice degree of freedom, σ are the vector of spin Pauli matrices, and τ_0 and σ_0 are identity matrices. The last two terms of (18) with a common coefficient ΔS are spin dependent and represent umklapp and normal scatterings, respectively. Pumping currents are related to the coefficients in (18) which dependent on the above-mentioned spin-mixing conductance. This conductance is determined by the scattering matrices with spin flip on the N/AF interface.

Although the AF resonance frequency attains the THz region (1 ~ 10 meV), the motion of the staggered field remains adiabatic. The spin eigenstates and the scattering matrix (18) adiabatically adapt to the instantaneous configuration of AFs. Regarding the staggered field l and the magnetization m as two independent adiabatic parameters [24, 27, 28], the pumped spin current I_s with the scattering matrix(18) can be obtained in the form

$$I_s = \frac{e}{\hbar}\left[G_r(l \times \dot{l} + m \times \dot{m}) - G_i \dot{m} \right] \qquad (19)$$

This expression arises from a coherent sum of two independent spin pumping contributions by m_1 and m_2. Due to the mixing of scattering channels from different magnetic sublattices, the spin-mixing conductance G_r and G_i are different from those of F. Moreover, AF dynamics is much faster than F that corresponds to a stronger spin pumping.

By taking a time average of(19) over one period of oscillation, only the first two terms survive and contribute to the dc component of spin current I_s^{dc}. Despite that $|m| \ll |l|$, the contribution of $m \times \dot{m}$ to I_s^{dc} can be comparable to that of $l \times \dot{l}$. This is because I_s^{dc} is proportional to the cone angle θ^2 of precessionand the cone angle associated with the staggered field is much smaller than the one associated with the magnetization, $\theta_l \approx 0$ but $\theta_m \approx \pi/2$.

From the sublattice degree of freedom involved in the AF dynamics it is follows a staggered spin pumping. A staggered spin current represents the imbalance between the spin current carried by the two sublattices. It has three components $I_{ss}^{(i)}$ ($i = 1,2,3$) from which the component

$$\frac{e}{\hbar} I_{ss}^{(3)} = G_r(l \times \dot{m} + m \times \dot{l}) - G_i \dot{l} \qquad (20)$$

only survives. Elastic scattering in the normal metal will destroy any staggered spin accumulation, which decays on the time scale of $\hbar/t$. Therefore, the staggered spin current is defined within a distance of the mean free path away from the interface.

The reciprocal effect of spin pumping is STT, which describes the back action that a spin current exerts on the AF. In linear response, an AF is driven by two thermodynamic forces $f_l = -\delta F / \delta l$ and $f_m = -\delta F / \delta m$ (energy dimension), where

$$F = \frac{\hbar}{2} \int dv \left[\frac{\omega_0}{a^2} m^2 + \frac{\omega_l}{a\omega_H} \sum_i (\partial_i l)^2 - \omega_H H \cdot m \right] \qquad (21)$$

is the free energy. Here $\omega_0 = \omega_A + 2\omega_E$ and ω_l are the homogeneous and inhomogeneous exchange frequencies, respectively. Enforced by $m \cdot l = 0$ and $(l)^2 \approx 1$, the symmetry allowed dynamics described by the system [25, 26]

$$\hbar \dot{l} = (a^3/v) f_m \times l \qquad (22a)$$

$$\hbar \dot{m} = (a^3/v) f_l \times l + f_m \times m, \qquad (22b)$$

Where v is the system volume. Inserting them into (20) gives the response of the spin current to f_m and f_l. Invoking the Onsager reciprocity relation, we derive the response of l and m to a given spin voltage V_s in the normal metal, which are identified as two STT terms T_l and T_m. To linear order in m

$$T_l = -\frac{a^3}{ev}\left[G_r l \times (m \times V_s) - G_i l \times V_s \right],$$
$$T_m = -\frac{a^3}{ev} G_r n \times (m \times V_s), \qquad (23)$$

that treats STTs on the two sublattices as completely independent.

In solving the AF dynamics, it is instructive to eliminate m and derive a closed equation of motion in terms of l alone [27-30]. In the linear approximation in V_s, m, and $\partial_t l$ the effective dynamics is described by the equation

$$l \times (\ddot{l} + \alpha\omega_0 \dot{l} + \omega_R^2 l_\perp) = \frac{\omega_0 a^3 G_r}{ev} l \times l \times V_s \qquad (24)$$

where α is the Gilbert damping constant, and $l_\perp$ are perpendicular components of l with respect to the easy axis. Since the STT only acts on the interface fora thin AF film a possible nonuniform motion of l is disregarded..

At small enough V_s collinear with the easy axis, the solution for a spectrum of (24) characterizes by a negative imaginary part of the frequency ω so that any perturbed motion will decay exponentially in time and the system is stable. However, a sufficiently large V_s flips the sign $\text{Im}\,\omega$, which makes the system unstable and marks the onset of uniform AF excitation. The condition $\text{Im}[\omega] = 0$ determines the threshold spin voltage $V_s^{th} = \pm(ev\alpha\omega_l)/(a^3 G_r)$, where $+(-)$ corresponds to the excitation of the right-handed (left-handed) mode.

5. Dynamic Feedback in AF/SH Structures

In the framework the current-induced dynamics of insulating antiferromagnets in a spin Hall geometry, sufficiently large in-plane currents perpendicular to the Néel AF order can trigger spontaneous oscillations at frequencies between the acoustic and the optical eigenmodes [17, 23, 26]. The direction of the driving current determines the chirality of the excitation. When the current exceeds a threshold, the combined effect of current-induced torques and spin pumping introduces a dynamic feedback that sustains steady-state oscillations with amplitudes controllable via the applied current. This permits to obtain the SH nano-oscillator with operating frequencies in THz range.

When an applied STT compensates the magnetic damping, the magnetization becomes unstable: it either switches to another direction or evolves into a steady-state oscillation. While the former improves writing operations in magnetic memory devices, the latter enables sustainable ac signal generation from dc inputs, giving rise to spin-torque oscillators (STOs) [31, 32]. In ferromagnets, currents or magnetic fields can tune the STO output frequency from the MHz to the GHz regime.

STOs can potentially be operated at much higher THz frequencies when antiferromagnets (AFs) replace ferromagnets. It is possibly owing to the THz range of the eigenfrequencies of typical AFs and possibility of spontaneous excitations of an AF by an anti-damping STTs. While most AFs are insulators where STTs cannot be operated by passing through a current, the SHE can produce STTs even when electrons do not flow through the magnet [31]. Therefore, integrating STOs with the SHE paves the way towards low-dissipation spin Hall nanooscillators (SHNOs) [6].

However, to realize AF-based SHNOs, current-induced excitations should not grow indefinitely, but instead should evolve into steady-state oscillations and generate a substantial ac output. Although an AF under the action of an anti-damping STT does not suffer magnetic switching, its Néel AF vector experiences either no dynamics or a right-angle precession around the direction of the spin accumulation [18]. Since the oscillation amplitude is not continuously tunable via the applied current, the device does not meet the requirements of an SHNO.

Steady-state oscillations are realizable in ferromagnetic STOs for the following reasons. In a spin-valve device, the angle dependence of the Gilbert damping and that of the anti-damping STT differ. As a result, when the driving current is above the threshold, there exists a unique angle where the two competing effects compensate. Then, a steady-state oscillation is stabilized at that angle. However, this features no longer active where the SHE creates the anti-damping STT. Therefore, one needs to introduce alternative mechanisms to prevent a spontaneous excitation from growing into magnetic switching.

Solution of the mentioned problem is based on the use of a feedback mechanism [17] that is realizable in an AF/heavy-metal heterostructure. The feedback effect originates from the combined effect of the SHE and its reverse process that connects the spin pumping with the spin backflow [33, 34], which is independent of the dipolar interaction. The threshold of spontaneous excitations is determined via solving the AF order dynamics in the linear response regime. The correlation between the threshold and a current density is related to the SHE in the heavy metal. The feedback is indispensable to sustain uniform auto-oscillations. Herewith, THz SHNO generates a substantial ac voltage output with its amplitude continuously tunable via the applied dc current.

Characteristic properties of magnetic dynamics of the AF in device geometry in Fig. 5 can be described in the framework of two-sublattice crystal structure with the magnetizations vectors m_1 and m_2. The magnetic dynamics is characterized by the AF vector $l = (m_1 - m_2)/2$ and the small magnetization $m = (m_1 + m_2)/2$, and angular frequencies $\omega_\perp$, $\omega_\parallel$ and ω_E corresponding to the hard axis, easy plane anisotropy and the Heisenberg exchange interaction, respectively. In the macrospin description, the free energy is

$$F = -\hbar\omega_3 l^2 - \hbar \sum_{i=1,2} \frac{\omega_i}{2}\left((r_i l)^2 + (r_i m)^2\right) \qquad (25)$$

where $\omega_3 = (\omega_E + \omega_\perp)$, $\omega_1(\omega_2) = \omega_\parallel(\omega_\perp)$ and $r_{1(2)} = x(z)$, which defines thermodynamic forces, $\hbar f_{l(m)} = -\partial F/\partial l(m)$. The coupled equations of motion are

$$\dot{l} = f_2 \cdot (m, l) + \alpha(m \times \dot{l} + l \times \dot{m}) + T_l \qquad (26a)$$

$$\dot{m} = f_1 \cdot (m, l) + \alpha(m \times \dot{m} + l \times \dot{l}) + T_m \qquad (26b)$$

where $f_{1(2)} = (f_{m(l)}\times, f_{l(m)}\times)$ (where $\times$ denotes the vector multiplication), α is the Gilbert damping constant, andthe STTs given by [13,21]

$$T_m = l \times (\omega_s \times l) + m \times (\omega_s \times m),$$
$$T_l = l \times (\omega_s \times m) + m \times (\omega_s \times l). \qquad (27)$$

Here the STT strength is determines via the vector of spin accumulation ω_s.

The vector decomposition $l = x + l_\perp \exp(i\omega t)$ in (26) results in the eigenfrequencies expression

$$\omega_\pm = i\omega_E \alpha + \left[\omega_E^2 \omega' \pm \omega_E \sqrt{\omega_\perp^2 - 4\omega_s^2}\right]^{1/2} \qquad (28)$$

where $\omega' = \omega_\perp + 2\omega_\parallel - \alpha^2$, + (-) denotes the optical (acoustic) mode. As ω_s increase, the real parts $\mathrm{Re}[\omega_+]$ and $\mathrm{Re}[\omega_-]$ approach each other until they become degenerate at $\omega_s = \omega_\perp/2$. The imaginary parts $\mathrm{Im}[\omega_+]$ and $\mathrm{Im}[\omega_-]$ remain degenerate and unaffectedfor $\omega_s < \omega_\perp/2$. When $\omega_s > \omega_\perp/2$,

$\text{Im}[\omega_+]$ ($\text{Im}[\omega_-]$) reduces (grows) rapidly, indicating that the damping is diminished (enhanced) by the STT.
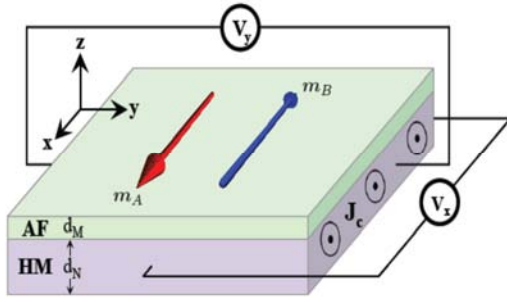
Figure 5. *An insulating AF/HM heterostructure. The applied dc current density J_c drives the AF via the SHE. The dynamics of the AF pumps spin current back into N, and converts into electric field via the ISHE, which is monitored by two voltmeters.*

At the threshold [18],

$$\omega_s^{th} = \sqrt{\frac{\omega_\perp^2}{4} + \alpha^2 (2\omega_\parallel + \omega_\perp)\omega_E} \qquad (29)$$

$\text{Im}[\omega_+]$ vanishes, which marks the onset of spontaneous excitation of the optical mode and the breakdown of the linear response approximation. The uniaxial symmetry enforces that $\text{Im}[\omega_+]$ also vanishes for the threshold so that the auto-oscillation can be triggered by a reversed current as well.

In the absence of the hard-axis anisotropy, the threshold (29) is linear in α, so the anti-damping effect occurs when the STT is turned on. However, in the general case where $\omega_\perp > 0$, the anti-damping effect appears only when $\omega_s > \omega_\perp / 2$. Vectors m_1 and m_2 always exhibit opposite chiralities, i.e., they rotates counterclockwise (clock-wise). However, at the degenerate point $\omega_s = \omega_\perp / 2$, the chirality of m_1 (m_2) in the optical (acoustic) mode reverses. At $\omega_s > \omega_\perp / 2$, both m_1 and m_2, hence the Néel vector l, all acquire the same chirality. At the threshold ω_s^{th}, the excited optical mode is right-handed. If ω_s changes sign, the optical mode is still excited, but its chirality becomes left-handed. These suggest that the direction of the current determines the chirality of the excitation.

In the considered two-layered nanostructure, insulating AF/heavy normal metal (HM) with strong spin-orbit coupling (Fig. 5) a current density J_c is applied along the y-direction perpendicularly to the AF vector l. The SHE in the HM generates anti-damping STTs to drive the AF vector dynamics, which in turn pumps spin current back into the HM. The pumped spin current converts into a charge voltage due to the inverse SHE. The spin diffusion equation in the presence of the SHE under boundary conditions involving both spin-pumping and STT, results in the expression

$$J_c^{th} = \omega_c^{th} \frac{d_M (h\sigma + 2\lambda e^2 G_r \coth\frac{d_N}{\lambda})}{2\theta_s \alpha^3 \lambda e G_r \tanh\frac{d_N}{\lambda}} \qquad (30)$$

describing the dependence of the a critical current density on the threshold STT (29), the spin Hall angle θ_s, and the areal density of transverse mixing conductance G_r. From (30) it is follows that the critical current density J_c^{th} can be lowered by reducing (increasing) the thickness of the AF d_M (HM d_N).

The sustained steady-state oscillation of the AF vector in the mentioned nanostructure can be realized via the dynamic feedback effect. The pumped spin current from a precessing AF vector into the HM experiences a backflow [33, 34]. In HMs, however, the spin pumping and the spin backflow are also connected via the combined effect of the SHE and its inverse process, which feeds the Néel vector dynamics back into itself. In ferromagnets, such a feedback mechanism manifests as a nonlinear damping effect in the magnetization dynamics. Similar feedback-induced damping effect can occur for AFs. In this case, the pumped spin current into the HM converts into an electric field E due to ISHE. According to Ohm's law,

$$J_c = \sigma E - \theta_s (\sigma / 2e) z \times \partial_z \boldsymbol{\mu}_s \qquad (31)$$

where $\boldsymbol{\mu}_s$ is the spin accumulation in the HM. At the fixed current density J_c through external circuits, a change of the electric field E necessarily leads to a change of the spin accumulation. Subsequently, the change of $\boldsymbol{\mu}_s$ diffuses and generates an additional spin current, which will finally deliver the influence of spin pumping back into the AF vector through STTs. Closing such a feedback loop results in a feedback torque. should be added to (27) as

$$T_{FB} = \alpha_{NL} \left[l_z^2 l \times \dot{l} - \dot{l}_z (z \times l) \right] \qquad (32)$$

where the feedback coefficient is

$$a_{NL} = \frac{\theta_s^2 \alpha^3}{d_M} \frac{2\hbar\lambda e^2 G_r^2 \coth\frac{d_N}{\lambda}}{(h\sigma + 2\lambda e^2 G_r \coth\frac{d_N}{\lambda})} \qquad (33)$$

While the feedback effect seems to be a higher order effect as a_{NL} is proportional to θ_s^2, it can be significantly enhanced by searching for materials with large θ_s. The feedback-induced nonlinear damping is a critical ingredient because it dramatically modifies the dynamical behavior of an SHNO using AF.

A salient feature of the considered stable oscillation phase is that the applied DC current density J_c controls the output power and that the output power is substantial that is indispensable for an SHNO. In the stable oscillation phase, the actual frequency output lies between the acoustic and the optical modes. The AC voltage output is determined by ISHE and the spin pumping. For a fixed J_c the total electric field

$E = J_c / \sigma + \Delta E$ includes a time varying part

$$\Delta E = \frac{\theta_s \hbar}{d_N} \frac{\lambda e G_r \tanh \frac{d_N}{2\lambda}}{h\sigma - 2\lambda e^2 G_r \coth \frac{d_N}{\lambda}} (\boldsymbol{l} \times \dot{\boldsymbol{i}}) \times \boldsymbol{z} \qquad (34)$$

A time average results in the effective value of the components $\bar{E}_x$ and $\bar{E}_y$ which are appreciably large in the stable oscillation phase.

6. SH Magnetoresistance in Nanostructures

Interconnection between the magnetic dynamics in magnetic layers and the charge current in the adjacent nonmagnetic heavy metal (HM) nanolayers with the strong spin-orbit interaction can exhibit via the so-called the spin Hall magnetoresistance effect (SME) [35, 36] of the magnetic-induced change of the charge current. The impact of the magnetic dynamics on the charge current in nonmagnetic layers is related to the conversion of the spin current magnetic induced in HM into the transverse charge current by the ISHE. The impact of the charge current on the magnetic states occurs via its SHE conversion into the transverse spin accumulation and the spin torque force.

Especially clearly, SME is exhibited in the case of insulating magnetic (IM) nanolayer (specifically, yttrium iron garnet (YIG)) adjusting to the HM nanolayer (specifically, Pt) possessing by the strong enough spin-orbit interaction. In such the nanostructure the change in resistance due to SMR is related to a combination of the SHE and ISHE, acting simultaneously [37, 38]. When a charge-current J_e is sent through a Pt nanolayer, a transverse spin-current J_s is generated by the SHE following $J_e \propto \sigma \times J_s$, where σ is the polarization direction of the spin-current. Part of this created spin-current is directed towards the interface as is shown in Fig. 6.
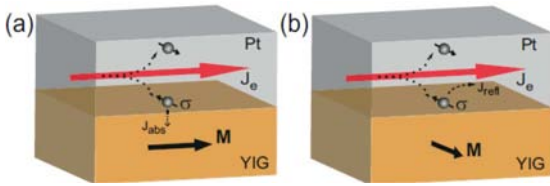
Figure 6. *Schematic of the passage of spin and charge currents at the SMR in a YIG/Pt nanostructure. (a) When the magnetization $\boldsymbol{M}$ YIG is perpendicular to the spin polarization $\boldsymbol{\sigma}$ of the spin accumulation created in the Pt by the SHE, the spin accumulation will be absorbed ($\boldsymbol{J}_{abs}$) by the localized moments in the YIG. (b) For $\boldsymbol{M}$ parallel to $\boldsymbol{\sigma}$, the spin accumulation cannot be absorbed, which results in a reflected spin-current back into the Pt, where an additional charge-current $\boldsymbol{J}_{refl}$ will be created by the ISHE.*

At the interface, the electrons in the Pt will interact with the localized moments in the YIG. Depending on the magnetization (M) direction of the YIG, electron spins will be absorbed ($M \perp \sigma$) or reflected ($M \parallel \sigma$). By changing the

direction of the magnetization of the YIG, the polarization direction of the reflected spins, and thus the direction of the additional created charge-current, can be controlled. A charge-current with a component in the direction perpendicular to J_e can also be created, which generates a transverse voltage.

In a diffusion approximation for both magnetic and HM nanolayers the spin and charge currents are expressed in terms of gradients of charge and spin accumulations (or spin-dependent electrochemical potentials and densities). The charge current density is the expectation value of the current operator $j = e(n\boldsymbol{v} + \boldsymbol{v}n)/2$, where e is the electron charge, n is the electron density, and $\boldsymbol{v}$ is the velocity operator. For a normal metal with constant density n_N and rift velocity v_N, $j_{eN} = en_N v_N$. The spin current in the non-relativistic limit is the second-order tensor

$$\overleftrightarrow{j}_{sN} = \frac{e}{2} \langle j \otimes \sigma + \sigma \otimes j \rangle = \left(j_{sx}, j_{sy}, j_{sz} \right)^T \qquad (35)$$

where σ is the vector of Pauli spin matrices, and $\langle \cdots \rangle$ denotes an expectation value. The row vectors $j_{si} = en(\boldsymbol{v}\sigma_i + \sigma_i \boldsymbol{v})/2$ are the spin current densities polarized in the i-direction. In metallic ferromagnets with homogenous texture, the average spin current is projected along the unit vector of the magnetization direction $\boldsymbol{m}$, so the charge current and spin current tensor have the form

$$\begin{aligned} j_{cF} &= e(n_{\uparrow F} \boldsymbol{v}_{\uparrow F} + n_{\downarrow F} \boldsymbol{v}_{\downarrow F}), \\ \overleftrightarrow{j}_{sF} &= j_{sF} \otimes \boldsymbol{m} = (j_{\uparrow F} - j_{\downarrow F}) \otimes \boldsymbol{m}, \end{aligned} \qquad (36)$$

where j_{cF} is the spin current density direction vector, "$\otimes$" denotes that the polarization is locked along $\boldsymbol{m}$. In contrast to the charge current, the spin current is not conserved in the presence of the spin-orbit interaction and non-collinear magnetizations, leading to spin-transfer to the lattice or magnetization, respectively.

Inthe diffusion approach for the two-current model currents close to the interface of the heterostructure are determined via gradients of the spin-dependent chemical potentials $\mu_{\varsigma F}$, $j_{\varsigma F} = -(\sigma_{\varsigma F}/e) \times \nabla \mu_{\varsigma F}$, where $\varsigma = (\uparrow, \downarrow)$ represents the spin direction along of the magnetization and $\sigma_{\varsigma F}$ is the spin-dependent conductivity. The charge and spin currents $j_{cF} = j_{\uparrow F} + j_{\downarrow F}$ and $j_{sF} = j_{\uparrow F} - j_{\downarrow F}$, respectively, are expressed via charge and spin chemical potentials $\mu_{cF} = (\mu_{\uparrow F} + \mu_{\downarrow F})/2$ and $\mu_{sF} = (\mu_{\uparrow F} - \mu_{\downarrow F})/2$, respectively, in the form of the form of Ohm's law [37]

$$j_{cF(sF)} = -\frac{\sigma_F}{e} \left[1(P)\nabla \mu_{cF} + P(1)\nabla \mu_{cF} \right] \qquad (37)$$

Where $P = (\sigma_{\uparrow F} - \sigma_{\uparrow F})/(\sigma_{\uparrow F} + \sigma_{\uparrow F})$ is the conductance spin polarization, $\sigma_F = \sigma_{\uparrow F} + \sigma_{\downarrow F}$ is the total conductivity. The mentioned potentials are determined by the diffusion equations

$$\nabla^2 \mu_{sF} = \frac{\mu_{sF}}{\lambda_F^2}, \quad \nabla^2 (\mu_{cF} + P\mu_{sF}/2) = 0 \qquad (38)$$

where the spin-flip diffusion length $\lambda_F = (\lambda_{\uparrow F}^{-2} + \lambda_{\downarrow F}^{-2})^{-1/2}$ is expressed in terms of the spin-diffusion length $\lambda_{\varsigma F} = \sqrt{D_{\varsigma F} \tau_{sf,\varsigma F}}$ for each spin ($\tau_{\varsigma f,sF}$ is the spin-dependent spin-flip time). The spin-dependent charge diffusion constant $D_{\varsigma F} = \tau_{\varsigma F} v_{\varsigma F}^2 /3$ depends on the spin-dependent relaxation time $\tau_{\varsigma F}$ and Fermi velocity v_ς. Solutions of (38), corresponding to boundary conditions at interface, due to (37) determine the charge and spin currents.

In normal metals, the induced spin accumulations is represented by the (position dependent) vector $\boldsymbol{\mu}_{sN} = (\mu_{sx}, \mu_{sy}, \mu_{sz})^T - \mu_{cN}\mathbf{1}$, components of which together with the charge chemical potential obey the diffusion equation system

$$\nabla^2 \mu_{si} = \frac{\mu_{si}}{\lambda^2}, \quad \nabla^2 \mu_{cN} = 0 \qquad (39)$$

Without the SHE, charge and spin currents express by the system

$$\boldsymbol{j}_{cN} = -\frac{\sigma_{cN}}{e}\nabla\mu_{cN}, \quad \boldsymbol{j}_{si} = -\frac{\sigma_{si}}{e}\nabla\mu_{si} \qquad (40)$$

The spin polarization in the case of the NM layers has arbitrary direction in contrast to the case of the magnetic layers.

In the considered case of the bilayer nanostructure HM/FI (FI denotes insulating magnetic) represented in Fig. 7, in which the charge current flow in the metal parallel to the applied electric field $\boldsymbol{E}$ and the SHE generate a spin accumulation, generalization of the Ohm's law (37) can be represented by the system [19]

$$\boldsymbol{j}_{si} = \frac{\sigma_N}{e}\left(\theta_S \boldsymbol{x}_i \times \nabla\mu_{cN} + \frac{1}{2}\nabla\mu_{sx_i}\right) \qquad (41)$$

$$\boldsymbol{j}_{cN} = \frac{\sigma_N}{e}\left(\nabla\mu_{cN} + \frac{\theta_S}{2}\sum_i \boldsymbol{x}_i \times \nabla\mu_{sx_i}\right) \qquad (42)$$

Where $\boldsymbol{\mu}_{sN} = (\mu_{sx}, \mu_{sy}, \mu_{sz})^T - \mu_{cN}\mathbf{1}$ is the spin accumulation, i.e. the spin-dependent chemical potential relative to the charge chemical potential $\mu_{cN} = e\varphi$, σ_N is the electric conductivity,
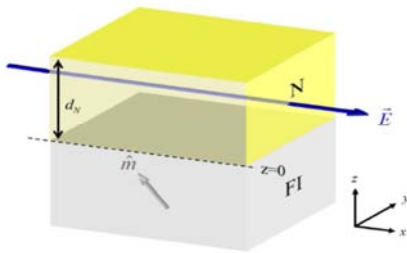
and "×" denotes the vector cross product operating on the gradients of the spin-dependent chemical potentials. The SHE is represented by the first term in (6.7) that generates the spin currents parallel to the applied electric field $\boldsymbol{E} = E_x \boldsymbol{x}$ (Fig. 7). The ISHE is governed by the second term in (42) that connects the gradients of the spin accumulations to the charge current density.

According to (41) and (42), the spin current in N consists of conventional diffusion and spin Hall drift contributions. The spin current density flowing in the z-direction is described by the expression

$$\boldsymbol{j}_{sz} = -\frac{\sigma_N}{2e}\nabla_z\boldsymbol{\mu}_{sN} - j_{s0}^{SH}\boldsymbol{y} \qquad (43)$$

where $j_{s0}^{SH} = \theta_S \sigma_N E_x$ is the bare spin Hall current, i.e., the spin current generated directly by the SHE. Due to the boundary conditions $\boldsymbol{j}_{sz}(z)$ is continuous at the interfaces ($z = d_N, 0$). The spin current density at a vacuum interface ($z = d_N$) vanishes, while at the magnetic interface ($z = 0$), it is governed by the spin accumulation and spin-mixing conductance according to (2), $\boldsymbol{j}_{sz}(0) = -\boldsymbol{j}_s^{(N|F)}$. Due to (39) with mentioned boundary conditions, the spin accumulation due describes by the relation

$$\frac{\boldsymbol{\mu}_{sN}(z)}{\mu_s^0} = -\boldsymbol{y}\frac{\sinh A(z)}{\sinh A(0)} - \frac{2\lambda \cosh B(z)}{\sinh B(0)} \times [\boldsymbol{m}\times(\boldsymbol{m}\times\boldsymbol{y})\operatorname{Re} + (\boldsymbol{m}\times\boldsymbol{y})\operatorname{Im}]\varphi(G_{\uparrow\downarrow}) \quad (44)$$

where $A(z)$ and $B(z)$ were defined in (12), and $\varphi(z) = z(\sigma_N + 2\lambda z \coth B(2d_N))^{-1}$, μ_s^0 is the spin accumulation at the interface in the absence of spin-transfer. From (44) it follows the distribution spin current in N

$$\frac{\boldsymbol{j}_s^z(z)}{j_{s0}^{SH}} = \boldsymbol{y}\left(\Delta_1(z) - 1\right) - \Delta_2(z)\,\mathbf{R}\,\varphi(G_{\uparrow\downarrow}) \qquad (45)$$

where

$$\Delta_1(z) = \frac{\cosh A(z)}{\cosh A(0)}, \quad \Delta_2(z) = \frac{2\lambda \tanh A(0)\sinh B(z)}{\sinh B(0)},$$

$\mathbf{R}$ denotes the expression emphasized by squared brackets in (44). The spin current at the interface N|F vanishes when the magnetization is along $\boldsymbol{y}$. The spin current at the interface and the torque on the magnetization are activated, while the spin accumulation is dissipated under rotation of the magnetization from $\boldsymbol{y}$ to $\boldsymbol{x}$, the spin current at the interface N|F, while the spin accumulation is dissipated correspondently. The $\boldsymbol{x}$-components of both spin accumulation and spin current vanish when the magnetization is along $\boldsymbol{x}$ and $\boldsymbol{y}$, and are largest at $(\boldsymbol{x}+\boldsymbol{y})/2$.

The ISHE drives a change current in the $x-y$ plane by the diffusion spin current component flowing along $\boldsymbol{y}$-direction. The total longitudinal (along x) and transverse (along $\boldsymbol{y}$) charge currents [37]

$$\frac{j_{cx}(z)}{\sigma_N E_x} = 1 + \theta_S^2\left[\Lambda_1(z) + (1 - m_y^2)\Lambda_2(z)\operatorname{Re}\varphi(G_{\uparrow\downarrow})\right] \qquad (46)$$

$$\frac{j_{cy}(z)}{\sigma_N E_x} = \theta_S^2 \Lambda_2 (1 - m_y^2) \left[m_x m_y \operatorname{Re} - m_z \operatorname{Im} \right] \varphi(G_{\uparrow\downarrow}) \qquad (47)$$

describe the magnetization dependence of the charge current.

Averaging (46) and (47) over the thickness z results in the corresponding electrical resistances, which in the first-order approximation in θ_S^2 describe the magnetization dependence [37]

$$\rho_x = \rho - \frac{\theta_{SH}^2 \tanh A(0)}{A(0)} \left(1 - \frac{\lambda(1 - m_y^2)\tanh A(0)}{2} \operatorname{Re}\varphi(G_{\uparrow\downarrow}) \right) \qquad (48)$$

$$\rho_y = -\frac{\theta_S^2 \lambda \tanh^2 A(0)}{A(0)} \left(m_x m_y \operatorname{Re} - m_z \operatorname{Im} \right) \varphi(G_{\uparrow\downarrow}) \qquad (49)$$

Here, when the N layer thickness increases relatively to the spin-flip diffusion length ($\lambda / d_N \to 0$) $A(0) \to 0$ and SMR effect vanishes. The SMR magnitude is proportional to the second power of the spin Hall angle) and it is related to the spin-mixing conductance) at the interface which is determined by the spin-dependent electron scattering.

References

[1] Equation Chapter 1 Section 1L. Zutic, J. Fabian, and S. Sarma, "Spintronics: Fundamentals and applications," Rev. Mod. Phys., vol. 76, pp. 323-413, April 2004.

[2] J.Manchon, H.C. Koo, J. Nitta, S. M. Frolov, and R.A. Duine, "New Perspective for Rashba Spin-Orbit Coupling," Nature Materials, vol. 36, pp. 871-882, August 2015.

[3] A. Hoffmann, "Spin Hall Effects in Metals," IEEE Trans. Magn., vol. 49, pp. 5172-5193, October 2013.

[4] Y. Tserkovnyak, A. Brataas, G. E. Bauer, and B. I. Halperin, "Nonlocal magnetization dynamics in ferromagnetic heterostructures," Rev. Mod. Phys., vol. 77, pp. 1375-1421, October 2005.

[5] E. R. J. Edwards, H. Ulrichs, V. E. Demidov, S. O. Demokritov, and S. Urazhdin, "Parametric excitation of magnetization oscillations controlled by pure spin current," Phys. Rev. B, vol.86, pp. 134220-134230, October 2012.

[6] L. Liu, C.-F. Pai, Y. Li, D. C. Ralph, and R. A. Buhrman, "Spin-Torque Switching with the Giant Spin Hall Effect of Tantalum," Science, vol. 336, pp. 555-558, May 2012.

[7] R. H. Liu, W. L. Lim, and S. Urazhdin, "Spectral Characteristics of the Microwave Emission by the Spin Hall Nano-oscillator," Phys. Rev. Lett., vol. 110, pp. 147601-147605, April 2013.

[8] D. Baither, G. Schmitz, and S.O. Demokritov, "Magnetic nanooscillators driven by pure spin current.," Nature Mater., vol. 11, pp. 1028–1031, December 2012.

[9] T. Yang, T. Kimura, and Y, Otani, "Giant spin-accumulation signal and pure spin-current-induced reversible magnetization switching," Nature Phys., vol. 4, pp. 851-854, October 2008.

[10] N. Ebrahim-Zaden, and S Urazhdin, "Optimization of Pt-based spin-Hall effect spintronic devices," Appl. Phys. Lett., vol.102, pp. 132402-132411, April 2013.

[11] N. V. Volkov. PHYS-USP, "Spintronics: manganite-based magnetic tunnel structures," vol. 55, pp. 250-269, March 2012.

[12] J. E. Hirsch, "Spin Hall effect," Phys. Rev. Lett., vol. 83, pp. 1834-1837, August 1999.

[13] E. M. Chudnovsky, "Theory of spin Hall effect," Phys. Rev. Lett., vol. 99, pp. 206601-206604, November 2007.

[14] I. M. Miron, G. Gaudin, S. Auffer, A. Bodmacq, A. Schuhl, S. Pizzini, J. Vogel, and P. Gambardalla, "Current-driven spin torque induced by the Rashba effect in ferromagnetic metal layer,"Nature Materials, vol. 9, pp. 230-234, January 2010.

[15] A. Manchon, and S. Zhang, "Theory of spin torque due to spin-orbit coupling," Phys. Rev. B., vol. 79, pp. 094422-1-0994422-8,March 2009.

[16] X. Wang, and A. Manchon, "Diffusive Spin Dynamics in Ferromagnetic Thin Films with a Rashba Interaction," Phys. Rev. Lett., vol. 108, pp. 117201-117205, March 2012.

[17] R. Cheng, J.-G. Zhu, and D. Xiao, "Dynamic Feedback in Ferromagnet/Spin-Hall Heterostructures," Phys Rev Lett., vol. 117, pp. 097202-097206, August 2016.

[18] H.V. Gomonay, and V. M. Loktev, "Spin transfer and current-induced switching in antiferromagnets," Phys. Rev. B, vol. 81, pp. 144427-144437, April 2010.

[19] A. Brataas, G. E. W. Bauer, and P. J. Kelly, "Non-collinear magnetoelectronics,"Phys. Rep., vol.427, pp. 157-256, April 2006..

[20] P. Gambardella, and I. M. Miron, "Current-induced spin-orbit torque," Phil. Trans. R. Soc. A, vol. 369, pp. 3175-3197, July 2011.

[21] Y. Ou, D. C. Ralph, and R. A. Buhrman, "Strong spin Hall effect in the antiferromagnetic PtMo," Phys. Rev. B, vol. 93, pp. 220405-22017, June 2016.

[22] K. Ando, S. Takahashi, K. Harii, K. Sasage, J. Ieda, S. Maekawa, and E. Saitoh, "Electric Manipulation of Spin Relaxation Using the Spin Hall Effect,"Phys. Rev. Lett., vol. 101, 036601-036613, July 2008.

[23] R. Cheng, D. Xiao, and A. Braatas, "Terahertz Antiferromagnetic Spin Hall Nano-Oscillator," Phys. Rev. Let., vol. 116,pp. 207603-207607, October 2015.

[24] Ya. Tserkovnyak, and S.A. Bender, "Spin Hall phenomenology of magnetic dynamics," Phys. Rev B, vol. 90, pp. 014428-014435, July 2014.

[25] Ya. Tserkovnyak, A. Brataas, and E.W. Bauer, "Spin pumping and magnetization dynamics in metallic multilayers," Phys. Rev. B, vol. 66, pp. 224403-224412, November 2002.

[26] R. Cheng, J. Xiao, Q. Niu, and A. Brataas, "Spin Pumping and Spin-Trasfer Torques in Antiferromagnets," Phys. Rev. Lett., vol. 113, pp. 057601-057614, July 2014.

[27] O. Mosendz, V. Vlaminck, J. E. Pearson, F. Y. Fradin, G. E. W. Bauer, S. D. Bader, and A. Hoffmann, "Detection and quantification of inverse spin Hall effect from spin pumping in permalloy/normal metal bilayers," Phys. Rev. B, vol. 82, pp. 214403-214415, December 2010.

[28] P.W. Brouwer, "Scattering approach to parametric pumping," Phys. Rev. B, vol. 58, pp. R10135-R10139, October 1998.

[29] V. E. Demidov, S. Urazhdin, H. Ulrichs, V. Tiberkevich, A. Slavin, D. Baither, G. Schmitz, and S.O. Demokritov, "Magnetic nano-oscillator driven by pure spin current," Nature Materials, vol. 11, pp. 1028-1031, December 2012.

[30] C.-F. Pai, L. Liu, H. W. Tseng, D. C. Ralph, and R. A. Buhram, "Spin transfer torque devices utilizing the giant spin Hall effect of tungsten," Appl. Phys. Lett., vol. 101, pp. 082407-082415, November 2012.

[31] K.-W. Kim, J.-H. Moon., K.-J. Lee, and H.-W. Lee, "Prediction of Giant Spin Motive Force due to Rashba Spin-Orbit Coupling," Phys. Rev. Lett., vol. 108, pp. 21722-21731, May 2012.

[32] C. H. Wong, and Ya. Tserkovnyak, "Hydrodynamic theory of coupled current and magnetization dynamics in spin-textured ferromagnets," Phys. Rev. B, vol.80, pp. 184411-184421, November 2009.

[33] H. L. Wang, C. H. Du, Y. Pu, R. Adur, P. C. Hammel, and F. Y. Yang, "Scaling of Spin Hall Angle in 3d, 4d and 5d Metals from $Y_3Fe_5O_{12}$/Metals Spin Pumping," Phys Rev. Lett., vol. 112, pp. 197201-197207, May 2014.

[34] A. Brataas, Ya. Tserkovnyak, and E. W. Bauer, and B.I. Halperin, "Spin battery operated by ferromagnetic resonance," Phys. Rev. B, vol. 66, pp. 060404-060407, February 2002.

[35] N. Vlietstra, J. Shan, V. Castel, B. J. van Wees, and J. B. Youssef, "Spin-Hall magnetoresistance in platinum on yttrium iron garnet: Dependence on platinum thickness and in-plane/out-of-plane magnetization," Phys. Rev. B, vol. 87, pp. 184421-184433, May2013.

[36] H. Nakayama, M. Althammer, Y.-T. Chen, K. Uchida, Y. Kajiwara, D. Kikuchi, T. Ohtani, S. Geprägs, M. Opel, S. Takahashi. R. Gross, G. E. W. Bauer, S.T.B. Goennenwein, and E. Saitoh, "Spin Hall Magnetoresistance Induced by a Nonequilibrium Proximity Effect," Phys. Rev. Lett., vol. 110, pp. 206601-206614, May 2013.

[37] Y. T. Chen, S. Takahashi, H. Nakayama, M. Althammer, S. T. B Goennenwein, E. Saitoh, and G. E. W. Bauer, "Theory of spin Hall magnetoresistance," Phys. Rev. B, vol. 87, pp. 14411-14424, February 2013.

[38] M. B. Jungfleisch, V. Lauer, R. Neb, A. V. Chumak, and B. Hillebrands, "Improvement of the yttrium iron garnet /platinum interface for spin pumping-based," Appl. Phys. Lett., vol. 103, pp. 022411-022423, July 2013.